Nano Today 59 (2024) 102502

Contents lists available at ScienceDirect

Nano Today

journal homepage: www.elsevier.com/locate/nanotoday

Calibrated absolute optical contrast for high-throughput characterization of horizontally aligned carbon nanotube arrays

Yue Li [a,b], Ying Xie [a], Jianping Wang [c], Yang Xu [b], Shurui Wang [a,c], Yunbiao Zhao [b], Liu Qian [a,*], Ziqiang Zhao [a,b,**], Jin Zhang [a,c,**]

[a] School of Materials Science and Engineering, Peking University, Beijing 100871, China
[b] State Key Laboratory of Nuclear Physics and Technology, School of Physics, Peking University, Beijing 100871, China
[c] Beijing Science and Engineering Center for Nanocarbons, Beijing National Laboratory for Molecular Sciences, College of Chemistry and Molecular Engineering, Peking University, Beijing 100871, China

ARTICLE INFO

Keywords:
Carbon nanotube array
Absolute optical contrast
Calibration
Differential principles
High-throughput characterization

ABSTRACT

Horizontally aligned carbon nanotube (HACNT) arrays hold significant potential for various applications in nanoelectronics and material science. However, their high-throughput characterization remains challenging due to the lack of methods with both high efficiency and high accuracy. Here, we present a novel technique, Calibrated Absolute Optical Contrast (CAOC), achieved through the implementation of differential principles to filter out stray signals and high-resolution calibration to endow optical contrast with physical significance. CAOC offers major advantages over previous characterization techniques, providing consistent and reliable measurements of HACNT array density with high throughput and non-destructive assessment. To validate its utility, we demonstrate wafer-scale uniformity assessment by rapid density mapping. This technique not only facilitates the practical evaluation of HACNT arrays but also provides insights into balancing high throughput and high resolution in nanomaterial characterization.

Introduction

Horizontally aligned carbon nanotube (HACNT) arrays have garnered significant interest due to their unique physical and chemical properties, which are highly beneficial for applications in nanoelectronics, sensors, and composite materials [1–5]. Over the past few decades, the focus has shifted from laboratory research to practical applications, revealing challenges in achieving uniformity and stability at the wafer scale using traditional fabrication methods [6]. To overcome these bottlenecks, it is crucial to develop characterization techniques that provide efficient and accurate feedback for experimental optimization. Traditional methods such as scanning electron microscopy (SEM), atomic force microscopy (AFM), and transmission electron microscopy (TEM) are precise but time-consuming and limited in throughput [7–9]. Therefore, there is a pressing need for a high-throughput, non-destructive technique to accurately characterize HACNT arrays.

Optical characterization offers high throughput and has been widely used in fields such as defect detection in electronics [10], biomedical imaging [11], and material science [12,13]. However, the nanoscale properties of carbon nanotubes (CNTs) result in an extremely limited scattering cross-section in optical characterization [14,15], with contrast levels around 10^{-4}. Fortunately, the one-dimensional structure of CNTs results in a strong depolarization effect, allowing their optical contrast to be enhanced by two orders of magnitude under appropriate polarized optical settings [15,16]. Based on this principle, optical imaging and spectroscopy techniques of individual CNT were developed, which enabled complete chirality profiling with high-throughput [14,17]. Furthermore, optical imaging coupled with in-situ growth were employed to study the dynamic process of individual CNT growth, significantly advancing our understanding of CNTs [16,18,19]. Although significant progress has been made, characterization of HACNT arrays still faces substantial challenges. Individual CNTs exhibit a lateral broadening of several micrometers in polarized optical characterization, making it impossible to resolve HACNT arrays with a density greater than 1 tube/μm. In our previous work, we demonstrated

* Corresponding author.
** Corresponding authors at: School of Materials Science and Engineering, Peking University, Beijing 100871, China.
E-mail addresses: qianliu-cnc@pku.edu.cn (L. Qian), zqzhao@pku.edu.cn (Z. Zhao), jinzhang@pku.edu.cn (J. Zhang).

https://doi.org/10.1016/j.nantod.2024.102502
Received 13 July 2024; Received in revised form 5 September 2024; Accepted 11 September 2024
Available online 14 September 2024

the use of polarized optical characterization for HACNT arrays [20]. Despite its high throughput, the measurement accuracy was inadequate for practical applications. One major reason is the relative nature of contrast measurements, especially when transparent substrates like sapphire or quartz are used, where stray light from the substrate interferes with the CNT contrast. Additionally, we used the absorption cross-section of carbon atoms and the average diameter of CNTs to derive the density from optical contrast without considering the complexity of the actual optical path, which led to deviations from the real density. Therefore, to improve the accuracy of characterization based on the advantages of the high throughput of optical methods, we need to establish a more accurate correlation between density and optical contrast.

In this study, we introduce the Calibrated Absolute Optical Contrast (CAOC) method, a novel approach designed to address these challenges. First, we incorporated the angle between the HACNT arrays and the polarizer as a degree of freedom and obtained the optical contrast of CNTs. Using the differential principle, we extracted the cross terms between the CNTs and the substrate, naturally filtering out stray signals other than those from the CNTs. Due to its measurement consistency, we refer to this as absolute optical contrast (AOC). Furthermore, we calibrated the AOC using characterization techniques that can achieve single-tube resolution, establishing an absolute calibration function between density and AOC. This method significantly improves the characterization efficiency of HACNT arrays by approximately 10^3 times, enabling high-throughput, wafer-scale sample analysis while maintaining the density measurement accuracy of high-resolution techniques.

Results and discussion

Fig. 1a shows the experimental setup for characterizing HACNT arrays using polarized optical microscopy. The light source passes through the first polarizer (P_1) and illuminates the sample surface. Theoretically, the CNT-scattered electric field (E_{NT}) is polarized along the CNT direction due to a strong depolarization effect on light polarized

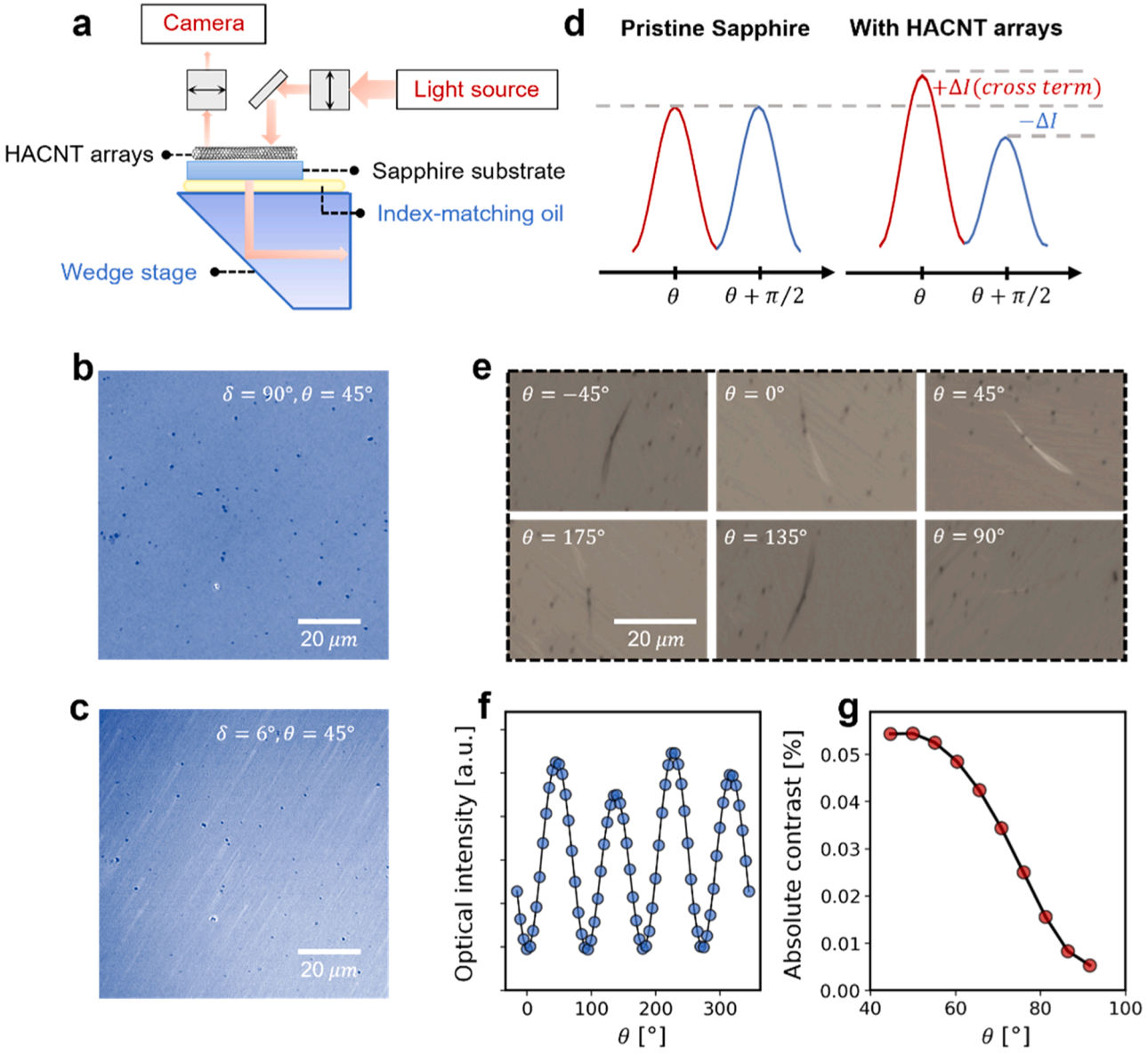

Fig. 1. (a) Experimental setup for characterizing HACNT arrays using polarized optical microscopy. (b) Optical microscope image of HACNT arrays under non-polarized conditions. (c) Optical microscope image of HACNT arrays under optimally polarized conditions, showing enhanced CNT contrast. (d) Principle of absolute contrast measurement. (e) Dark-to-bright transition of a CNT bundle as the orientation angle θ changes. (f) Intensity-angle spectrum of HACNT arrays. (g) Absolute contrast results calculated using Eq. 3 based on the fitted data from (f).

perpendicularly to the CNT, while the substrate reflection (E_R) retains the polarization of P_1. Therefore, by setting P_2 perpendicular to P_1, substrate reflection is significantly reduced while preferentially retaining the CNT reflection, thus enhancing the contrast of the CNTs ($\Delta I/I_R$). As shown in Eq. 1[17], since $|E_{NT}|^2$ is extremely small, the contrast contribution mainly arises from the cross term. Hence, P_1 and P_2 need to be set at a small angle δ deviating from 90° to amplify the signal of the cross term. Experimentally, it was found that when δ is approximately ± 6°, the CNT contrast is maximized.

$$\frac{\Delta I}{I_R} = \frac{|E_R + E_{NT}|^2 - |E_R|^2}{|E_R|^2} = \frac{2|E_R|\cdot|E_{NT}|}{|E_R|^2} \tag{1}$$

During the preparation of HACNT arrays, a-plane sapphire or ST-cut quartz substrates are typically employed for directional growth. Consequently, the impact of these transparent substrates, which exhibit polarization responses, must be considered during characterization. Reflections from the upper surface of the substrate maintain the polarization direction, whereas reflections from the lower surface undergo a polarization shift after traversing the substrate, thus escaping the cross-polarization setup and introducing substantial background signals [16]. To mitigate this issue, index-matching oil was utilized to eliminate interface reflections, and a wedge structure was employed to deflect the light, ensuring the CNT contrast remains at the order of 10^{-2}. This approach facilitates non-transfer characterization, which is essential for non-destructive sample testing. Fig. 1b and c present optical microscope images of the same region under non-polarized and optimally polarized conditions, respectively, demonstrating a marked enhancement in CNT contrast with this optical configuration.

The polarized optical setup enables the visualization of HACNT arrays using an optical microscope, however, accurate measurement of optical contrast is essential for quantitative characterization. Traditionally, contrast measurement relied on Eq. 2, which requires separately measuring both the total optical intensity (I_T) and the substrate optical intensity (I_R) to calculate the optical contrast ($\Delta I/I_R$). This method is suitable for single CNT or low-density arrays, but for high-density arrays, where CNTs fully cover the optical field of view, it necessitates the destructive process of scraping off nanotubes to create a substrate region (Figure S1). Additionally, the complexity of transparent substrates often results in measurement errors, preventing accurate and consistent assessment of HACNT array optical contrast.

$$\frac{\Delta I}{I_R} = \frac{I_T - I_R}{I_R} \tag{2}$$

To address these issues, we introduced the CNT orientation angle θ as a degree of freedom. By rotating the sample stage, an intensity-angle spectrum was obtained. Theoretically, the substrate signal exhibits a periodicity of $\pi/2$, while the cross-term signal between the substrate and CNTs displays a periodicity of π, changing sign every 90°. Fig. 1d illustrates this principle. The intensity-angle spectrum of pristine sapphire shows highly consistent $\pi/2$ periodic peaks, whereas samples containing HACNT arrays exhibit differences in peak heights, indicating the contribution of the cross-term, which is the primary source of CNT contrast (see Figure S2 and Supplementary Note 1). Fig. 1e visually demonstrates this process, showing the dark-to-bright transition of a CNT bundle as θ changes. By processing the brightest and darkest points of the CNTs, other signals outside the CNTs can be naturally eliminated, yielding the absolute contrast of CNTs. Fig. 1f shows the actual measurement results of the HACNT array contrast spectrum, with peaks consistent with the theoretical predictions. Fig. 1g presents the contrast result calculated using Eq. 3 based on the fitted data from Fig. 1f. This method allows for the measurement of HACNT array contrast without separately measuring the background, significantly reducing measurement errors (Figure S3).

$$\frac{\Delta I}{I_R} = \frac{I_T(\theta) - I_T(\theta + \pi/2)}{I_T(\theta) + I_T(\theta + \pi/2)} \tag{3}$$

AOC provides the theoretical basis for quantitatively characterizing HACNT arrays. In previous work, the absorption cross-section per carbon atom and the average diameter of the CNTs were used to correlate optical contrast with density [20]. However, this method is based on certain idealized assumptions, and the relationship between optical contrast and density necessitates further investigation. To address this, AOC was calibrated using high-resolution characterization techniques. Fig. 2 illustrates the calibration workflow, which primarily consists of two steps. First, we performed optical imaging at different angles, extracted the average brightness information from the images, and used Eq. 3 to obtain the AOC. Fig. 2a shows optical images of HACNT arrays at two intensity peak positions, where the bright-to-dark transition is visible within the dashed boxes.

Subsequently, the same regions of the samples were characterized using AFM or SEM to count the number of CNTs. To ensure the feasibility of the calibration, the scales of the optical and high-resolution characterizations were unified. For instance, in AFM characterization, a scale of 2 μm was selected, and 25 consecutive images were taken to correspond to the information extracted from a 50 μm optical image. To enhance the efficiency and accuracy of CNT counting, a computer vision (CV) program was developed to identify and count the CNTs. Fig. 2b visualizes the identification process, and Fig. 2c presents the AFM results for a 50 μm region, with the horizontal axis representing the coordinates of the CNTs and the vertical axis representing the CNT count. The overall consistency of the slope indicates the uniformity of the sample. This figure can be infinitely magnified, as shown in the insets. Notably, using this method, the coordinates of each CNT can be recorded, similar to the infinite zoom of satellite imagery. This method also evaluates the uniformity of CNT pitch. Figure S4 shows the pitch distribution of the CNTs obtained using “satellite imagery”, which follows a log-normal distribution with a mean value and standard deviation of 20.52 nm and 12.22 nm, respectively. This precise characterization and analysis method may potentially facilitate the application of CNTs in carbon-based electronics.

By integrating AOC with "satellite imagery", the function between the exact density and optical contrast of HACNT arrays can be determined. As shown in Fig. 3a, the data points are derived from four different samples, with Sample 1 being a pristine sapphire. A strong linear relationship ($R^2 = 0.98$) is observed, consistent with previous reports [20]. In contrast, using the method based on Eq. 2 to calculate optical contrast, the calibration (Figure S5) shows that while the density and contrast of each sample are individually linearly correlated, there is no unified calibration relationship. This further underscores the consistency and reliability advantage of AOC.

The accuracy of the measurements was subsequently evaluated. Errors primarily stem from two sources: the accuracy of CNT identification by CV programs and the accuracy of the calibration curve. Fig. 3b assesses the accuracy of CNT identification using 70 AFM images, with CNT quantity counted by both human scientists and CV programs (referred to as AI). The data points mostly fall on the y = x line, indicating the reliability of AI in density counting. Fifty points were selected to evaluate the accuracy of CAOC in density characterization. The horizontal axis represents the density results measured by AFM, while the vertical axis represents the density results measured by CAOC. As shown in Fig. 3c and S6, CAOC demonstrates overall good accuracy in density measurement, with larger errors in the low-density region (up to approximately 20 %) and minimal errors in the high-density region. Given that the CNT signals are relatively weak even under polarized settings, the accuracy of this method is significantly influenced by density. In essence, higher CNT density produces a stronger optical signal, which in turn increase the signal-to-noise ratio and enhances measurement accuracy. However, as the density decreases, the optical contrast signal gradually approaches the noise level, making it difficult to distinguish the CNT signal from noise, leading to a decline in accuracy.

A single AOC measurement requires taking 36 images, each with an

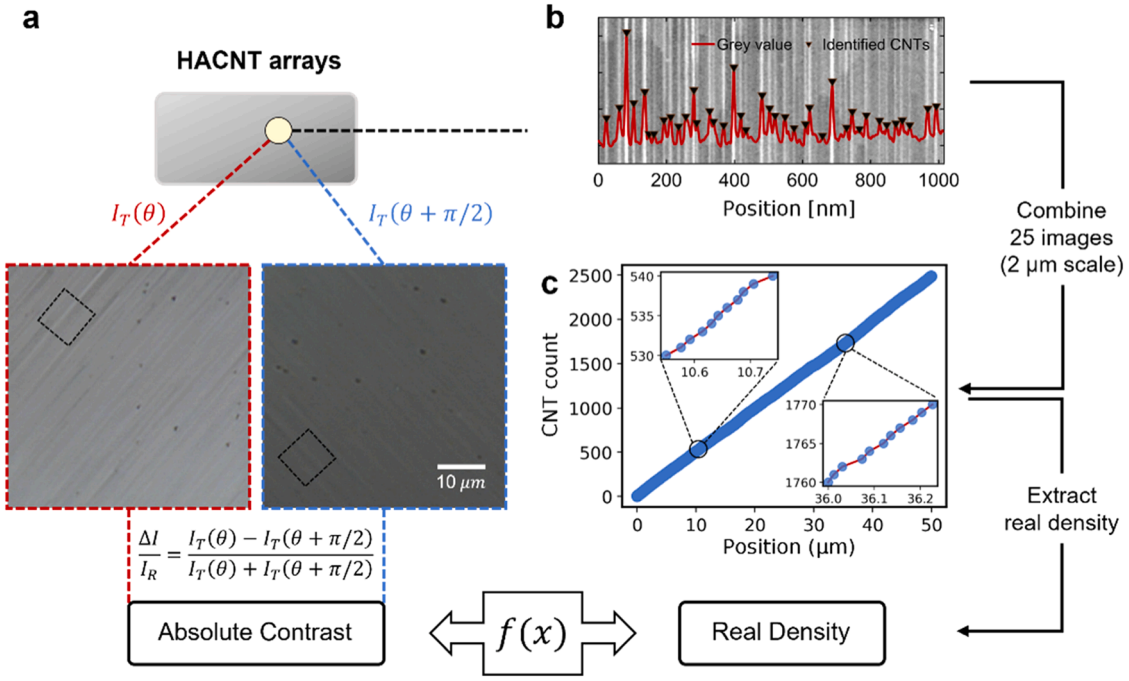

Fig. 2. (a) Optical images of HACNT arrays at two intensity peak positions, showing the bright-to-dark transition within the dashed boxes. (b) Visualization of the CNT identification process using a computer vision (CV) program. (c) AFM results for a 50 μm region, with the horizontal axis representing the coordinates of the CNTs and the vertical axis representing the CNT count. Insets demonstrate the zoom-in of two areas.

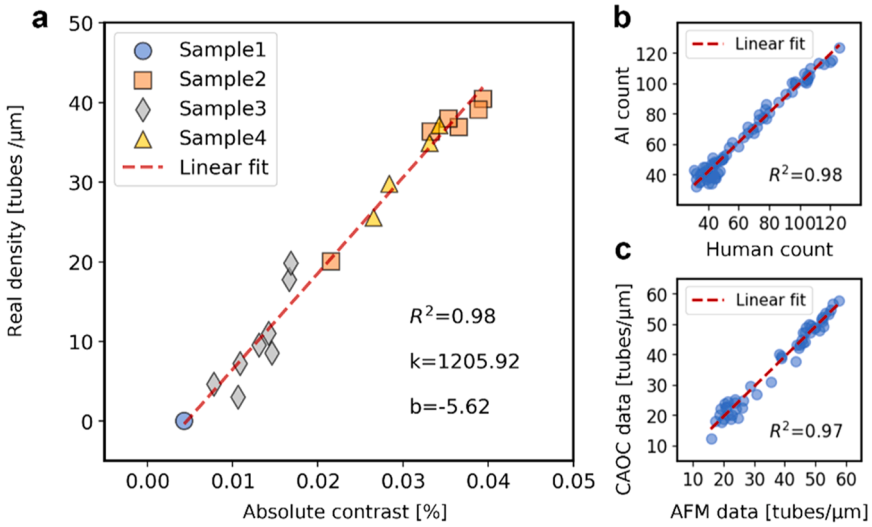

Fig. 3. (a) The relationship between AOC and the real density of HACNT arrays. Sample 1 is a pristine sapphire. (b) Assessment of CNT identification accuracy, with CNT quantities counted by both human scientists and CV programs (referred to as AI). (c) Evaluation of CAOC accuracy in density characterization, with the horizontal axis representing density results measured by AFM, and the vertical axis representing density results measured by CAOC.

integration time of 1 second. Considering the operator's handling time, one AOC point takes about 2 minutes. To further improve efficiency and support wafer-scale sample uniformity characterization, AOC was calibrated with optical intensity. For the same sample, during the same test (with consistent optical settings), I_R is a constant value, so theoretically, optical intensity is proportional to AOC (Eq. 4 and SI). The measurement efficiency of optical intensity is 36 times that of AOC. Therefore, by selecting 5 points on a sample for calibration (approximately 5 minutes), the efficiency of subsequent density measurements can be significantly improved. Based on this, a standardized density characterization process was developed, as illustrated in Fig. 4a:

$$I_T \propto \frac{\Delta I}{I_R} \tag{4}$$

1. High-throughput collection of optical intensity: Images of the HACNT array wafer were obtained using polarized optical microscopy with maximized CNT contrast. The average optical intensity was extracted from the central circular area (100 μm in diameter) of each image.
2. Calibration of the correlation between AOC and optical intensity: Five optical images were randomly selected, and the AOC in these regions was measured. The functional relationship between optical

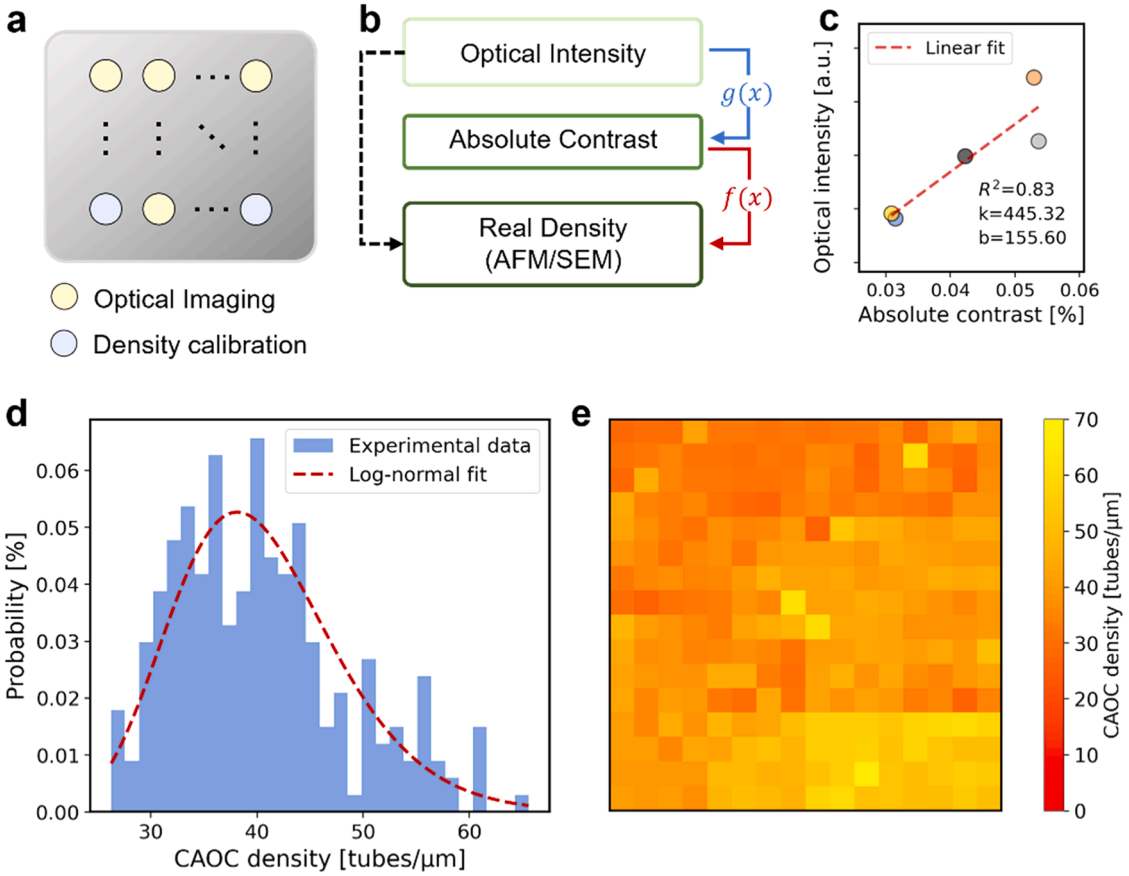

Fig. 4. (a) Schematic of the standardized density characterization process for HACNT arrays using optical imaging. (b) Relationship between optical intensity, AOC, and real density of HACNT arrays. (c) Calibration curve of the relationship between optical intensity and AOC. (d) Density distribution of a 1 cm × 1 cm HACNT array sample. (e) Density mapping of the 1 cm × 1 cm HACNT array sample.

intensity and AOC of HACNT arrays was obtained through linear fitting.

3. Density calculation and analysis: Using the absolute calibration function and the calibration function between AOC and optical intensity, all the optical intensities obtained in the first step were translated into HACNT array densities. This allowed us to statistically analyze the density uniformity of the HACNT-array wafer.

Fig. 4b illustrates the relationship between optical intensity, AOC, and actual density. Although the two calibration steps—from optical intensity to AOC and then to real density—can amplify experimental errors, this method significantly enhances efficiency, enabling practical assessment of wafer-scale density uniformity. Direct calibration between optical intensity and real density could further improve accuracy, but the calibration with high-resolution techniques required several hours.

Using this method, we characterized a 1 cm × 1 cm sample, uniformly selecting 144 (12×12) points across the sample and randomly choosing five points to measure AOC. The calibration curve is shown in Fig. 4c. Fig. 4d displays the density distribution of the entire sample, with an average density of approximately 40.40 tubes/μm and a standard deviation of about 7.95 tubes/μm. Fig. 4e is a mapping of the sample, illustrating that this method allows for rapid density partitioning, enabling the categorization of HACNT arrays for different applications. The entire characterization process took about 30 minutes, covering 1.44 % of the sample area. In contrast, AFM characterization in the same time would cover only about 10^{-5} of the area, lacking statistical significance. In terms of characterization efficiency, CAOC improves throughput by approximately three orders of magnitude compared to AFM.

Conclusion

In summary, we developed a CAOC method for high-throughput and accurate characterization of HACNT arrays. We proposed a novel approach for calculating the optical contrast of CNTs by utilizing the differential principle to naturally filter out stray signals, thereby obtaining experimentally consistent AOC. By integrating AOC with high-resolution techniques, we established a calibration function between AOC and real density, demonstrating a strong linear relationship consistent with theoretical predictions. The CAOC method enables practical assessment of wafer-scale density uniformity. Our standardized density characterization process allows for rapid and reliable density mapping of large-scale HACNT arrays. The ability to perform high-accuracy, non-destructive, and high-throughput density characterization represents a substantial advancement in the field of CNT, potentially accelerating the development of HACNT arrays and their applications. Moreover, the principle of using polarized optics and differential measurement to filter out stray signals is universal, and theoretically, it can be applied to various one-dimensional nanomaterials on different substrates, with only the calibration function needing fine-tuned.

However, the CAOC method has some limitations. For instance, it tends to have larger errors with low-density HACNT arrays, where optical contrast variations are minimal. This issue can be mitigated by using higher precision cameras. Additionally, AOC is not only related to density but also to the average diameter of CNTs[20]. Different growth methods may result in varying diameter distributions, necessitating extra calibration of the AOC-density function. Future work will focus on refining the technique to extend its applicability across a broader range

of CNT characterization. Overall, CAOC provides a powerful tool for the rapid and accurate characterization of HACNT arrays, and it also shows potential for application in other one-dimensional materials. The principles of differential measurement and calibration can solve the challenge of balancing high throughput with high accuracy, which is insightful for the development of nanomaterial characterization techniques, facilitating further research and development in nanotechnology.

Experimental section

Synthesis of HACNT arrays

HACNT arrays were grown on a-plane sapphire substrates. The catalyst was prepared by ion implantation, followed by carbon nanotube growth using a home-made vertical spraying chemical vapor deposition (VSCVD) system. The VSCVD system consists of a spray unit, a gas flow control system, and a dual-temperature heating chamber, which ensures uniform gas distribution and consistent sample exposure during the growth process. The typical operating temperature is 800–900 °C. Growth began with a flow of 300 standard cubic centimeters per minute (sccm) argon and 300 sccm hydrogen for 1–5 minutes to reduce Fe ions and form Fe nanoparticles in-situ. Subsequently, 10–20 sccm argon was introduced through an ethanol bubbler as the carbon feedstock. Throughout the process, argon flow was maintained at 300 sccm, and hydrogen flow varied from 300 to 500 sccm. The pressure remained at 70 Kpa, and the spraying distance was set at 10 mm.

General characterization

SEM images were obtained using a Hitachi S4800 SEM operated at 1.0 kV and 10 kV. Raman spectra of HACNT arrays with line mapping, conducted with a scan step of 5 μm and a laser beam spot of ~1 μm, were collected using a Jovin Yvon-Horiba LabRam system with 532 nm excitation. AFM images were obtained using a Dimension Icon microscope (Bruker).

Optical characterization

As shown in Fig. 1a, an optical microscope (Nikon Eclipse LV100N POL) equipped with a 10× objective (N.A. = 0.3, air), 40× objective (N.A. = 0.6, air), 100× objective (N.A. = 0.9, air), and a 50× objective (N.A. = 0.5, 22 mm long working distance), two polarizers (Nikon LV-PO), and a color camera (Nikon DS-Ri2) were used to capture the polarized optical images. One polarizer (P1) was located in the incident beam, and the second polarizer (P2) was placed in the reflective beam, allowing free rotation to change the analyzing direction with a rotation precision of 0.1°. A halogen lamp was used as the light source (Nikon LV-LH50PC). The aperture iris diaphragm and the field iris diaphragm enabled convenient control of the incident beam, with the field iris diaphragm used to eliminate excess light. For birefringent substrates, refractive index matching was performed to suppress the depolarized light from the back surface. The typical image exposure time was 1.0 s, with an analog gain of 14.0x.

Optical image processing

All characterized images were processed using custom-developed Python or MATLAB programs. CNT identification was primarily based on image enhancement and peak-finding algorithms. Optical image processing involved averaging the RGB intensity within masked regions. The specific code will be released on GitHub after peer review.

CRediT authorship contribution statement

Yue Li: Writing – original draft, Validation, Methodology, Investigation, Data curation, Conceptualization. **Ying Xie:** Resources, Methodology, Data curation. **Jianping Wang:** Validation, Methodology, Investigation, Formal analysis. **Yang Xu:** Resources, Methodology. **Shurui Wang:** Validation, Investigation. **Yunbiao Zhao:** Validation, Methodology. **Liu Qian:** Writing – review & editing, Validation, Supervision, Funding acquisition, Conceptualization. **Ziqiang Zhao:** Writing – review & editing, Supervision, Funding acquisition, Conceptualization. **Jin Zhang:** Writing – review & editing, Validation, Supervision, Resources, Funding acquisition, Conceptualization.

Declaration of Competing Interest

The authors declare that they have no known competing financial interests or personal relationships that could have appeared to influence the work reported in this paper.

Data availability

Data will be made available on request.

Acknowledgments

This work was financially supported by the Ministry of Science and Technology of China (2022YFA1203302), the National Natural Science Foundation of China (Grant Nos. 52021006, 52102032, 52272033), the Strategic Priority Research Program of CAS (XDB36030100), the Beijing National Laboratory for Molecular Sciences (BNLMS-CXTD-202001) and the Shenzhen Science and Technology Innovation Commission (KQTD20221101115627004).

Appendix A. Supporting information

Supplementary data associated with this article can be found in the online version at doi:10.1016/j.nantod.2024.102502.

References

[1] P. Avouris, M. Freitag, V. Perebeinos, Carbon-nanotube photonics and optoelectronics, Nat. Photon. 2 (2008) 341–350, https://doi.org/10.1038/nphoton.2008.94.
[2] M.F.L. De Volder, S.H. Tawfick, R.H. Baughman, A.J. Hart, Carbon nanotubes: present and future commercial applications, Science 339 (2013) 535–539, https://doi.org/10.1126/science.1222453.
[3] M. He, S. Zhang, J. Zhang, Horizontal single-walled carbon nanotube arrays: controlled synthesis, characterizations, and applications, Chem. Rev. 120 (2020) 12592–12684, https://doi.org/10.1021/acs.chemrev.0c00395.
[4] L. Liu, J. Han, L. Xu, J. Zhou, C. Zhao, S. Ding, H. Shi, M. Xiao, L. Ding, Z. Ma, C. Jin, Z. Zhang, L.-M. Peng, Aligned, high-density semiconducting carbon nanotube arrays for high-performance electronics, Science 368 (2020) 850–856, https://doi.org/10.1126/science.aba5980.
[5] D. Zhong, Z. Zhang, L. Ding, J. Han, M. Xiao, J. Si, L. Xu, C. Qiu, L.-M. Peng, Gigahertz integrated circuits based on carbon nanotube films, Nat. Electron. 1 (2017) 40–45, https://doi.org/10.1038/s41928-017-0003-y.
[6] Y. Xie, Y. Li, Z. Zhao, J. Zhang, Pave the way to the batch production of SWNT arrays for carbon-based electronic devices, Nano Res. 16 (2023) 12516–12530, https://doi.org/10.1007/s12274-023-6173-1.
[7] J. Li, Y. He, Y. Han, K. Liu, J. Wang, Q. Li, S. Fan, K. Jiang, Direct identification of metallic and semiconducting single-walled carbon nanotubes in scanning electron microscopy, Nano Lett. 12 (2012) 4095–4101, https://doi.org/10.1021/nl301561f.
[8] H. Ago, K. Nakamura, K. Ikeda, N. Uehara, N. Ishigami, M. Tsuji, Aligned growth of isolated single-walled carbon nanotubes programmed by atomic arrangement of substrate surface, Chem. Phys. Lett. 408 (2005) 433–438, https://doi.org/10.1016/j.cplett.2005.04.054.
[9] S. Zhang, L. Kang, X. Wang, L. Tong, L. Yang, Z. Wang, K. Qi, S. Deng, Q. Li, X. Bai, F. Ding, J. Zhang, Arrays of horizontal carbon nanotubes of controlled chirality grown using designed catalysts, Nature 543 (2017) 234–238, https://doi.org/10.1038/nature21051.
[10] J. Zhu, J. Liu, T. Xu, S. Yuan, Z. Zhang, H. Jiang, H. Gu, R. Zhou, S. Liu, Optical wafer defect inspection at the 10 nm technology node and beyond, Int. J. Extrem. Manuf. 4 (2022) 032001, https://doi.org/10.1088/2631-7990/ac64d7.
[11] C.W. Freudiger, W. Min, B.G. Saar, S. Lu, G.R. Holtom, C. He, J.C. Tsai, J.X. Kang, X.S. Xie, Label-free biomedical imaging with high sensitivity by stimulated Raman scattering microscopy, Science 322 (2008) 1857–1861, https://doi.org/10.1126/science.1165758.

[12] M. Celebrano, P. Kukura, A. Renn, V. Sandoghdar, Single-molecule imaging by optical absorption, Nat. Photon. 5 (2011) 95–98, https://doi.org/10.1038/nphoton.2010.290.
[13] P. Kukura, M. Celebrano, A. Renn, V. Sandoghdar, Imaging a single quantum dot when it is dark, Nano Lett. 9 (2009) 926–929, https://doi.org/10.1021/nl801735y.
[14] K. Liu, X. Hong, S. Choi, C. Jin, R.B. Capaz, J. Kim, W. Wang, X. Bai, S.G. Louie, E. Wang, F. Wang, Systematic determination of absolute absorption cross-section of individual carbon nanotubes, Proc. Natl. Acad. Sci. 111 (2014) 7564–7569, https://doi.org/10.1073/pnas.1318851111.
[15] J. Lefebvre, P. Finnie, Polarized light microscopy and spectroscopy of individual single-walled carbon nanotubes, Nano Res. 4 (2011) 788–794, https://doi.org/10.1007/s12274-011-0135-8.
[16] L. Monniello, H.-N. Tran, R. Vialla, G. Prévot, S. Tahir, T. Michel, V. Jourdain, Comprehensive model of the optical spectra of carbon nanotubes on a substrate by polarized microscopy, Phys. Rev. B 99 (2019) 115431, https://doi.org/10.1103/PhysRevB.99.115431.
[17] K. Liu, X. Hong, Q. Zhou, C. Jin, J. Li, W. Zhou, J. Liu, E. Wang, A. Zettl, F. Wang, High-throughput optical imaging and spectroscopy of individual carbon nanotubes in devices, Nat. Nanotechnol. 8 (2013) 917–922, https://doi.org/10.1038/nnano.2013.227.
[18] V. Pimonov, H.-N. Tran, L. Monniello, S. Tahir, T. Michel, R. Podor, M. Odorico, C. Bichara, V. Jourdain, Dynamic instability of individual carbon nanotube growth revealed by *In Situ* homodyne polarization microscopy, Nano Lett. 21 (2021) 8495–8502, https://doi.org/10.1021/acs.nanolett.1c03431.
[19] G.D. Förster, V. Pimonov, H.-N. Tran, S. Tahir, V. Jourdain, C. Bichara, Swinging crystal edge of growing carbon nanotubes, ACS Nano 17 (2023) 7135–7144, https://doi.org/10.1021/acsnano.2c07388.
[20] S. Deng, J. Tang, L. Kang, Y. Hu, F. Yao, Q. Zhao, S. Zhang, K. Liu, J. Zhang, High-throughput determination of statistical structure information for horizontal carbon nanotube arrays by optical imaging, Adv. Mater. 28 (2016) 2018–2023, https://doi.org/10.1002/adma.201505253.